ceramics

MDPI

Article

Reduction of Dewaxing and Sintering Time by Controlling the Particle Size of YSZ Particles for Stereolithography

Masaya Takahashi [1,*], Fiona Spirrett [2] and Soshu Kirihara [2]

[1] Graduate School of Engineering, Osaka University, Osaka 565-0871, Japan
[2] Joining and Welding Research Institute, Osaka University, Osaka 567-0047, Japan
* Correspondence: masaya-takahashi@jwri.osaka-u.ac.jp

Abstract: In ceramic stereolithography, composite "green" bodies must be thermally processed to de-bind organic content and sinter the material. The conventional process for dewaxing and sintering of yttria stabilized zirconia stereolithography components is typically very long. The time and energy cost of thermal treatment of these components can be reduced by controlling the size of the solid particles in the photosensitive material. The Discrete Element Method was used to model the number of particle contacts per mass using particles of various median diameter, and a three-dimensional curved surface graph was generated. Ceramic slurries were prepared using powders that fulfilled the conditions of various calculated data points from the DEM model analysis. The prepared slurries were processed by stereolithography additive manufacturing and fabricated precursors were thermally processed to dewax and sinter the parts. The relationship between the particle size and the occurrence of crack formation after heat treatment was investigated. Heat treatment parameters were further investigated using the predicted slurry composition that was optimal for crack prevention. The required time for dewaxing and sintering of yttria stabilized zirconia components was reduced to one tenth of the conventional time through optimization of slurry composition and thermal treatment schedule.

Keywords: yttria stabilized zirconia; sintering; stereolithography; discrete element method

check for updates

Citation: Takahashi, M.; Spirrett, F.; Kirihara, S. Reduction of Dewaxing and Sintering Time by Controlling the Particle Size of YSZ Particles for Stereolithography. *Ceramics* **2022**, *5*, 814–820. https://doi.org/10.3390/ceramics5040059

Academic Editor: Enrico Bernardo

Received: 30 September 2022
Accepted: 14 October 2022
Published: 18 October 2022

Publisher's Note: MDPI stays neutral with regard to jurisdictional claims in published maps and institutional affiliations.

Copyright: © 2022 by the authors. Licensee MDPI, Basel, Switzerland. This article is an open access article distributed under the terms and conditions of the Creative Commons Attribution (CC BY) license (https://creativecommons.org/licenses/by/4.0/).

1. Introduction

Yttria Stabilized Zirconia (YSZ) is used in a variety of applications, including artificial teeth [1], artificial joints [2] and solid electrolytes in fuel cells [3]. There are several methods for fabricating YSZ parts including Ceramic Injection Molding [4] (CIM) and press molding [5]. In recent years, research has been carried out on stereolithography to fabricate zirconia with complex shapes [6] and to make high-performance ceramic (HPC) parts [7]. In ceramic stereolithography, ceramic powder is mixed with a photo sensitive resin to form a slurry which is selectively cured by a UV laser to form 3D objects [8]. The composite precursors must be thermally heat treated to remove organic content and sinter to a dense ceramic part. Dewaxing and sintering of zirconia ceramics require a gradual increase in temperature over a long period of time to prevent microstructural growth and cracking [9]. This process is reported to take about 200 h [10], which must be reduced to improve operational efficiency and reduce power consumption [11]. The sintering temperatures of green bodies fabricated by stereolithography using YSZ particles, are reported to be 600 °C for de-binding, and 1550 °C for sintering [12]. The heating rate to the dewaxing temperature has been reported to be 0.83 °C/min, the temperature 3 °C/min and the dwell time 2.5 h [13,14].

The aim of this research was to reduce the dewaxing and sintering time of zirconia ceramic parts fabricated by stereolithography, by optimizing the material properties and thermal processing schedule. Specifically, controlling the ceramic particle size was expected to allow optimization of material properties for crack prevention during a faster thermal

post processing step. The Discrete Element Method (DEM) was used to predict solid particle interactions between simulated ceramic particles of defined particle size, and the model was used to create a three-dimensional surface graph to visualize the effect of particle size and standard deviation on particle contacts. The conditions identified by the DEM analysis were used to produce a ceramic slurry by mixing the corresponding particles in a photosensitive resin. The prepared slurry was used to produce disk-shaped samples by stereolithography, which were then subjected to a dewaxing and sintering process. The samples were observed after heat treatment and the materials most suited for short heat treatment were selected. Furthermore, using the selected particles, studies were conducted to reduce the dewaxing and sintering time by adjusting the heat treatment schedule.

2. Materials and Methods

2.1. Computational Modelling

The discrete element method was used for the characterization of ceramic particles. EDEM (Altair Engineering, Troy, MI, USA), a software designed for DEM analysis, was used to virtually simulate the particle locations of the ceramic after the dewaxing process. Data on the size distribution of hypothetical particles with median diameters and standard deviations between 0.1 and 0.9 μm were prepared. The analysis was carried out with the size of the particles set to 100 times the size of the particles to simplify the calculations. The standard deviation is defined as the square root of the mean of the square of the difference between each value and the mean. For a normal distribution, the mean ± standard deviation range would include 68% of the data. Simulations were conducted to fill cylindrical containers with each of these hypothetical particles. The containers were defined by a base radius of 1 mm and a height of 1 mm. The weight of the powder was defined as 8×10^{-3} g, the Poisson's ratio as 0.25 and the density as 6.05 g/cm^3, and the analysis was performed until all particles fell to the bottom of the cylinder due to gravity. These analyses determined the number of contact points of particles per weight in the container. A three-dimensional surface graph was then created, taking the median diameter, standard deviation, and the number of contact points of particles per weight as x, y, and z axes. The graph was created to visualize the effect of particle size and standard deviation on particle contacts. As the particle size distribution is not always symmetrical, the median diameter was adopted to represent the particle size distribution of the powder as opposed to the mean. Several points on a three-dimensional surface graph created from the analysis results were taken and the corresponding particles were used to prepare experimental materials to satisfy the conditions.

2.2. Material Preparation

Three types of Zirconia stabilized with Yttria particles at 3 mol% (3Y) and 4 mol% (4Y) with different particle size distributions were prepared: 3Y zirconia particles ("3Y-A", HSY-3F-J-LA, "3Y-B", HSY-3.0B, Daiichi Kigenso Kagaku Kogyo, Osaka, Japan) and 4Y zirconia particles ("4Y", HSY-0450, Daiichi Kigenso Kagaku Kogyo, Osaka, Japan). The median diameters were 0.48 μm, 0.87 μm and 0.16 μm, respectively. Powders 1–6 were prepared using these materials, satisfying the combinations of median diameter and standard deviation in Table 1 and Figure S1.

Slurries 1–6 were prepared by mixing the particles with a photosensitive resin (KC-1287, JSR, Tokyo, Japan) to form a paste with 42 vol.% solid content. The formed slurry was sealed in a container and thoroughly mixed in a planetary centrifugal mixer (SK-350T, Shashin Kagaku, Kyoto, Japan). Air bubbles were removed, and particles and resin were mixed simultaneously by centrifugal and shearing force during rotation and revolution. The rotation speed was approximately 1100 rpm and the revolution speed was approximately 800 rpm. The mixing process was repeated for each slurry using three sets of mixing parameters with a mixing time of 5 min.

Table 1. Material properties for YSZ powders (See Figure S1).

Material	Composition	Median Diameter (μm)	Standard Deviation (μm)	Particle Size Distribution (μm)
Powder/Slurry 1	3Y-A	0.48	0.19	0.2–1.0
Powder/Slurry 2	3Y-A + 3Y-B (5:1)	0.48	0.43	0.27–3.9
Powder/Slurry 3	3Y-A + 3Y-B + 4Y (7:2:1)	0.47	0.55	0.08–3.3
Powder/Slurry 4	3Y-A + 3Y-B (5:6)	0.62	0.67	0.27–3.9
Powder/Slurry 5	3Y-B + 4Y (10:1)	0.72	0.79	0.06–3.9
Powder/Slurry 6	3Y-B	0.87	0.69	0.27–5.0

2.3. Fabrication of YSZ Samples

YSZ samples were fabricated using a stereolithography system (SZ-2500, Shashin Kagaku, Kyoto, Japan) equipped with a 355 nm UV laser with a spot size diameter of 50 μm. A disk geometry with a height of 0.5 mm and a base diameter of 1.5 mm was fabricated. The continuous stereolithography process is schematically illustrated in Figure 1 [6]. The cross-sectional geometry was continuously formed by laser drawing on the slurry layers applied on the stage, with material solidifying by photo-polymerization. The solid object was successfully fabricated by layer lamination and bonding under optimized lithography conditions. The laser diameter and layer thickness were set at 50 μm, laser power at 150 mW and laser scan speed at 2000 mm/s.

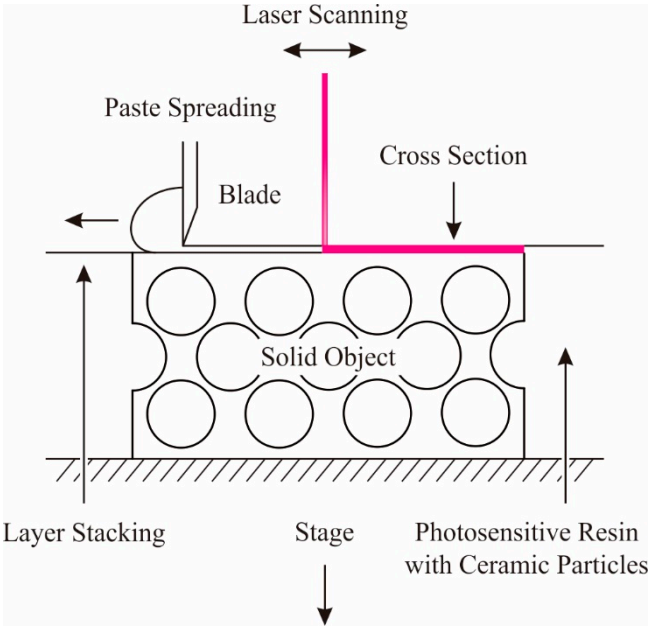

Figure 1. Schematic showing the stereolithography process. A UV laser scans 2D cross sections of the CAD model on layers of spread paste, which is then joined by photopolymerization and subsequent layer processing.

The heat treatment schedules investigated for dewaxing and sintering are shown in Table 2 and Figure 2. After dewaxing and sintering, each disk was examined for cracks and delamination. The presence or absence of cracks was considered to identify the optimal materials that would reduce the time required for dewaxing and sintering. The ceramic powders used to fabricate the samples that did not crack were selected, and slurries experimentally determined to have the maximum dispersion were mixed. The optimal slurry was used to fabricate disk samples, and post-process heat treatment schedule was investigated. A suitable temperature pattern for crack prevention and reduced processing time was explored. Heat treatment was applied to the 3D printed precursors using the combinations of dewaxing and sintering times in Table 2.

Table 2. Dewaxing and sintering time of heat treatment patterns.

Treatment Pattern	Dewaxing Heating Rate to 600 (°C/min)	Sintering Heating Rate to 1560 (°C/min)
A	1.0	3.0
B	0.3	3.0
C	0.4	6.0
D	0.5	6.0

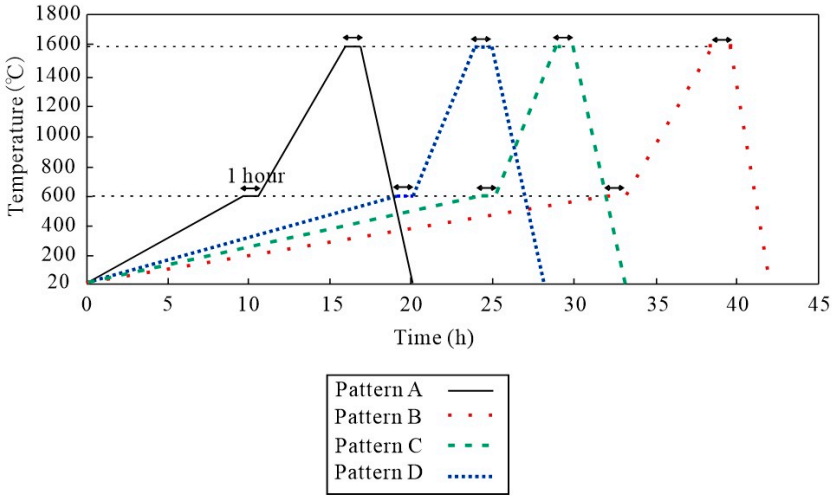

Figure 2. Graph showing the heat treatment schedules for YSZ samples. Patterns A–D show varying heating rates with isothermal holds at 600 °C and 1560 °C for 1 h.

Both the dewaxing and sintering processes were followed by a one-hour isothermal hold. The relative density of the sintered samples was measured using the Archimedes method and the microstructures were observed by SEM (JSM-6060, JEOL, Tokyo, Japan).

3. Results and Discussion

The results of the EDEM analysis are shown in Figure 3 (2D plots and coordinate data are available in Figure S2 and Table S1 of supplementary material). The larger the median diameter and standard deviation, the smaller the number of particle contacts per weight. The results of the dewaxing and sintering process for six different disk samples produced by stereolithography using Slurries 1–6 are described in the following text. Cracks and delamination were observed in Disks 1–3, but not in Disks 4–6. (Disks 1–6 refer to samples made using Powders 1–6.) The median particle diameters and standard deviations of powders 4–6 were larger than those of powders 1–3 and the number of contact points were smaller. The results suggest that slurries with particles with a large median diameter and standard deviation, and a low number of particle contact points can be sintered in a shorter time.

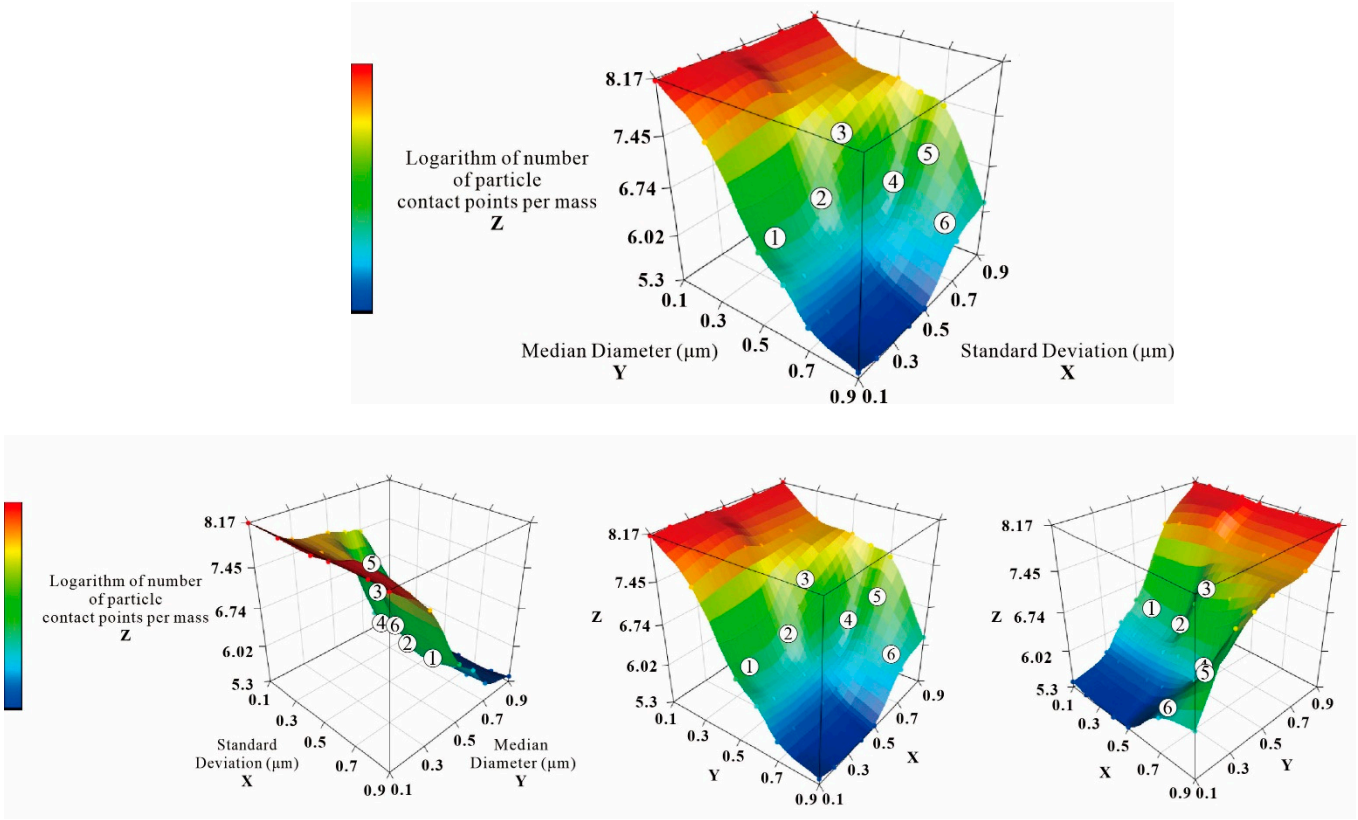

Figure 3. Various views of a 3D graph showing the relationship between median particle diameter (μm), standard deviation (μm) and logarithm number of particle contact points per mass (colored key represents the number of particle contact points per mass). The numbers 1–6 on the graph represent powders 1–6 (See Supplementary Material).

Further additions of Powder 5 and Powder 6 were made to Slurry 5 and Slurry 6, respectively, to maximize the particle dispersion ratio, as this is recommended for reduced sinter shrinkage, improved density, and good processability [15–18]. As a result, the maximum particle dispersion of Slurry 5 and Slurry 6 was 51 vol.% and 48 vol.%, respectively, resulting in pastes with a suitable viscosity for processing. A higher dispersion rate resulted in a shorter sintering time, with Slurry 5 requiring a shorter sintering time than Slurry 6.

The effect of the heat treatment schedule on sample cracking and delamination was observed. Cracking and surface delamination occurred in Pattern A, but was not observed in Patterns B-D. This suggests that the heating rate from room temperature to the dewaxing temperature had a significant impact on sample cracking. A faster heating rate was tolerated from dewaxing temperature to sintering temperature. The results of Pattern D showed that the heat treatment for these ceramic parts could be completed in about 1/10th (20 h) of the conventional dewaxing and sintering time.

Digital measurements of Disk 5′ revealed that the linear and volumetric shrinkage after dewaxing and sintering were estimated to be 19% and 50% respectively. (Disk 5′ is a disk prepared with 51 vol.% Slurry 5 and sintered with pattern D). The dewaxed and sintered ceramic samples were observed by SEM and Disk 5′ is shown in Figure 4. The observations were made at an acceleration voltage of 3 kV and a magnification of 500× and 20,000×. The microstructure of the zirconia was found to be sufficiently densified and relative density was determined to be 99.5%. Scanning Electron Microscopy confirmed that the fabricated parts had a dense, sintered microstructure.

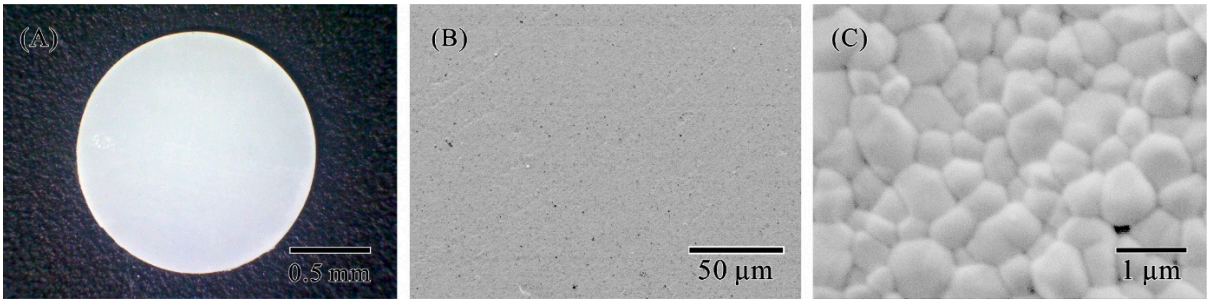

Figure 4. (**A**) photograph of the sintered zirconia ceramic sample (Disk5′), (**B**) SEM micrograph of Disk 5′ at 500× magnification, and (**C**) SEM micrograph of Disk 5′ at 20,000× magnification showing a dense microstructure.

4. Conclusions

Optimization of ceramic slurry composition successfully reduced the dewaxing and sintering time of yttria-stabilized zirconia to one-tenth of the conventional time. This reduction in dewaxing and sintering time is expected to save energy and improve the efficiency of the production process.

DEM was used to calculate the number of particle contacts per weight using simulated ceramic particles of varying median diameter and standard deviations. Several points on the three-dimensional surface graph from the simulation results were selected and slurries were prepared using particles satisfying these conditions. These slurries were used to produce disk-shaped samples by stereolithography additive manufacturing.

A 40-h dewaxing and sintering process was conducted on the disk samples. The two types of powder that did not crack were then selected and mixed with the photosensitive resin, and the maximum dispersion of zirconia particles in the slurry was identified as 48 vol.% and 51 vol.%, respectively. The slurry with 51 vol.% dispersion of zirconia particles was then subjected to a dewaxing and sintering process for around 20 h. SEM confirmed the densification of the microstructure.

In the DEM models described in this paper, a spherical morphology was used to represent the ceramic powder material. Future work will be carried out to generate a more accurate model using angular and irregular particles to represent the actual YSZ particle morphology. Future work will also include fabrication of YSZ parts with more complex geometries, observing the effect of particle size and heat treatment control on cracking.

Supplementary Materials: The following supporting information can be downloaded at: https://www.mdpi.com/article/10.3390/ceramics5040059/s1, Figure S1: Graphs showing particle size distribution of Powder1–6; Figure S2: 2D plots from the 3D graph showing logarithm of number of particle contact points per mass (z), standard deviation (x) and median diameter (y); Table S1: x, y, z coordinate data of powders 1-6 taken from the 3D graphical data.

Author Contributions: Conceptualization, S.K.; methodology, M.T. and S.K.; validation, M.T. and S.K.; formal analysis, M.T.; investigation, M.T.; resources, M.T.; data curation, M.T.; writing—original draft preparation, M.T.; writing—review and editing, F.S. and S.K.; visualization, M.T., F.S. and S.K.; supervision, S.K.; project administration, M.T. and S.K. All authors have read and agreed to the published version of the manuscript.

Funding: This research received no external funding.

Institutional Review Board Statement: Not applicable.

Informed Consent Statement: Not applicable.

Data Availability Statement: Not applicable.

Conflicts of Interest: The authors declare no conflict of interest.

References

1. Kontos, L.; Schille, C.; Schweizer, E.; Gerstorfer, G.J. Influence of surface treatment on the wear of solid zirconia. *Acta Odontol. Scand.* **2013**, *71*, 482–487. [CrossRef] [PubMed]
2. Fouletier, J.; Bonnat, M.; Bot, L.; Adamowicz, S.M. Calibration of a highly sensitive oxygen analyzer for biological applications using an oxygen pump. *Sens. Actuators B Chem.* **1997**, *45*, 155–160. [CrossRef]
3. Panthi, D.; Hedayat, N.; Du, Y. Densification behavior of yttria-stabilized zirconia powders for solid oxide fuel cell electrolytes. *J. Adv. Ceram.* **2018**, *7*, 325–335. [CrossRef]
4. Zainudin, M.; Ismail, M.; Shaari, N.; Manap, M.; Yahaya, M. Microstructural and Physical Properties of Yttria Stabilized Zirconia (YSZ) Prepared by Ceramic Injection Moulding (CIM). *J. Phys. Conf. Ser.* **2021**, *2051*, 012049. [CrossRef]
5. Kosmac, T.; Kocjan, A. Ageing of dental zirconia ceramics. *J. Eur. Ceram. Soc.* **2012**, *32*, 2613–2622. [CrossRef]
6. He, R.; Liu, W.; Wu, Z.; An, D.; Huang, M.; Wu, H.; Jiang, Q.; Ji, X.; Wu, S.; Xie, Z. Fabrication of complex-shaped zirconia ceramic parts via a DLP- stereolithography-based 3D printing method. *Ceram. Int.* **2018**, *44*, 3412–3416. [CrossRef]
7. Wang, J.; Dommati, H. Fabrication of zirconia ceramic parts by using solvent-based slurry stereolithography and sintering. *Int. J. Adv. Manuf. Technol.* **2018**, *98*, 1537–1546. [CrossRef]
8. Takahashi, M.; Kirihara, S. Stereolithographic Additive Manufacturing of Zirconia Electrodes with Dendritic Patterns for Aluminum Smelting. *Appl. Sci.* **2021**, *11*, 8168. [CrossRef]
9. Salamon, D.; Maca, K.; Shen, Z. Rapid sintering of crack-free zirconia ceramics by pressure-less spark plasma sintering. *Scr. Mater.* **2012**, *66*, 899–902. [CrossRef]
10. Nakamura, T.; Muto, N.; Nakahira, A. Development of Rapid Debinding Process and Debinding Behavior for Zirconia Molded Bodies Using Superheated Steam. *J. Soc. Powder Technol.* **2020**, *57*, 619–626. [CrossRef]
11. Watari, K.; Nagaoka, T.; Sato, K.; Hotta, Y. A strategy to reduce energy usage in ceramic fabrication—Novel binders and related processing technology—. *Synthesiology* **2009**, *2*, 137–146. [CrossRef]
12. Li, X.; Zhong, H.; Zhang, J.; Duan, Y.; Jiang, D. Fabrication of zirconia all-ceramic crown via DLP-based stereolithography. *Int. J. Appl. Ceram. Technol.* **2019**, *17*, 844–853. [CrossRef]
13. Ji, S.; Kim, D.; Park, M.; Yun, J. Sintering Process Optimization for 3YSZ Ceramic 3D-Printed Objects Manufactured by Stereolithography. *Nanomaterials* **2021**, *11*, 192. [CrossRef] [PubMed]
14. Camposilvan, E.; Marro, F.; Anglada, M. Enhanced reliability of yttria-stabilized zirconia for dental applications. *Acta Biomater.* **2015**, *17*, 36–46. [CrossRef] [PubMed]
15. Brady, A.; Grumman, N.; Chu, T.-M.G.; Halloran, J.W. Curing Behavior of Ceramic Resin for Stereolithography. In Proceedings of the Solid Freeform Fabrication Proceedings, Austin, TX, USA, 12–14 August 1996. [CrossRef]
16. Halloran, J.W. Ceramic Stereolithography: Additive Manufacturing for Ceramics by Photopolymerization. *Annu. Rev. Mater. Res.* **2016**, *46*, 19–40. [CrossRef]
17. Liu, W.; Li, M.; Nie, J.; Wang, C.; Li, W.; Xing, Z. Synergy of solid loading and printability of ceramic paste for optimized properties of alumina via stereolithography-based 3D printing. *J. Mater. Res. Technol.* **2020**, *9*, 11476–11483. [CrossRef]
18. Lakhdar, Y.; Tuck, C.; Binner, J.; Terry, A.; Goodridge, R. Additive Manufacturing of Advanced Ceramic Materials. *Prog. Mater. Sci.* **2021**, *116*, 100736. [CrossRef]